Exploring the performance of hybrid concentrated photovoltaic-thermoelectric systems: A multivariate assessment of system efficiency and material selection

Shuwen Hu[a], Dongxu Ji[a,*], Xiaoying Tang[a], Tao Ma[b], Jian Song[c,d], Christos N. Markides[d]

[a] *School of Science and Engineering, The Chinese University of Hong Kong, Shenzhen 518172, China*

[b] *School of Mechanical Engineering, Shanghai Jiao Tong University, Shanghai 200240, China*

[c] *Birmingham Centre for Energy Storage & School of Chemical Engineering, University of Birmingham, Birmingham B15 2TT, UK*

[d] *Clean Energy Processes (CEP) Laboratory, Department of Chemical Engineering, Imperial College London, London SW7 2AZ, UK*

Preprint not peer reviewed

This preprint research paper has not been peer reviewed. Electronic copy available at: https://ssrn.com/abstract=6589681

Exploring the performance of hybrid concentrated photovoltaic-thermoelectric systems: A multivariate assessment of system efficiency and material selection

Shuwen Hu[a], Dongxu Ji[a,*], Xiaoying Tang[a], Tao Ma[b], Jian Song[c,d], Christos N. Markides[d]

[a] *School of Science and Engineering, The Chinese University of Hong Kong, Shenzhen 518172, China*

[b] *School of Mechanical Engineering, Shanghai Jiao Tong University, Shanghai 200240, China*

[c] *Birmingham Centre for Energy Storage & School of Chemical Engineering, University of Birmingham, Birmingham B15 2TT, UK*

[d] *Clean Energy Processes (CEP) Laboratory, Department of Chemical Engineering, Imperial College London, London SW7 2AZ, UK*

Abstract

Hybrid concentrated photovoltaic–thermoelectric (CPV-TEG) systems have been proposed as a means to enhance solar energy utilization by recovering photovoltaic waste heat. However, their system-level performance under solar concentration remains debated, with existing studies reporting contradictory conclusions. In this work, a validated thermal-electrical model is employed to establish quantitative performance boundaries for hybrid CPV-TEG systems, through systematic comparison with standalone CPV configurations over a wide range of operating conditions. The effects of optical concentration ratio, cooling capacity, CPV cell characteristics, and thermoelectric (TE) material properties are examined. The results demonstrate that TEG integration does not provide net system-level benefits for silicon-based CPV cells across practical concentration ratios, due to temperature-induced efficiency degradation. In contrast, hybrid CPV-TEG systems become advantageous only within specific design regimes, characterized by medium-to-high concentration ratios, sufficiently strong thermal management, and CPV cells with low temperature coefficients. At a CR of 500, a hybrid system employing a low-efficiency, temperature-insensitive CPV cell achieves a 24% efficiency improvement over its standalone counterpart. Furthermore, a system-constrained material selection framework is applied to evaluate thermoelectric materials based on their coupled impact on system efficiency and photovoltaic operating temperature, enhancing the hybrid system efficiency to 41%. These results provide clear performance assessment and practical design guidance for hybrid CPV–TEG systems.

Keywords: concentrated photovoltaic; hybrid generation system; material selection; performance analysis; solar energy; thermoelectric generator

* Corresponding author. E-mail: jidongxu@cuhk.edu.cn (D. Ji).

Preprint not peer reviewed

This preprint research paper has not been peer reviewed. Electronic copy available at: https://ssrn.com/abstract=6589681

1. Introduction

Solar energy utilisation is commonly regarded as a promising solution to addressing the challenges associated with the scarcity of fossil fuels and environmental pollution, due to its significant advantages of abundance, affordability, and environmental sustainability. The conversion of solar energy into electricity through photovoltaic (PV) cells has become the most rapidly-developing technology within the solar energy sector. The power capacity increase of solar PV exceeded 370 GW in 2023, contributed to ~75% of the world's total renewable power capacity increment [1]. Despite the substantial growth in PV power generation globally, the efficiency of commercially prevalent silicon-based PV panels remains limited to 30%, due to inherent material properties [2], whereas a considerable portion of solar energy is dissipated as heat. To further improve the overall efficiency of solar energy utilization, it is of great importance to capture and reutilise the waste heat from PV panels.

A thermoelectric generator (TEG) is a solid-state device that has the ability to convert waste heat directly to electricity from the temperature difference applied across (i.e., between the hot and cold sides of) the device [3]. In Ref. [4] it was suggested that through optimization of a TEG's geometry and operational conditions, a TEG module can achieve efficiencies up to 10% for electricity generation. Therefore, and although the technology has some limitations relative to other waste heat recovery technologies, mainly arising from its reduced performance [5,6] and cost [3] viability in larger-scale applications [7], some the technology's merits (in particular, its modularity, lack of moving parts, seals, lubricants, working fluids, and leaks thereof [8]) may offer advantages when integrated within hybrid PV-TEG systems in smaller-scale, distributed applications.

In recent years, hybrid PV-TEG systems have been attracted increasing attention, with many efforts aimed at improving the overall electrical output and efficiency through operating parameters analysis and geometric optimization. Van Sark [9] developed a tandem-structure non-concentrated hybrid PV-TEG system, which assumed that the back side of the PV panel was fully covered with TEGs. The author simulated the system's performance under a solar irradiance lower than 1000 W/m^2 and reported that such roof-integrated PV-TEG modules could theoretically achieve an 8-23% efficiency increase if the figure of merit of thermoelectric materials could be further improved. research has focused on enhancing thermal gradients using copper concentrators [10] and reducing interface resistance through integrated, ceramic-free designs [11]. Modelling efforts have progressed from coupled environmental assessments in diverse climates [12] to advanced 2D unsteady-state simulations [13], including the use of

Preprint not peer reviewed

This preprint research paper has not been peer reviewed. Electronic copy available at: https://ssrn.com/abstract=6589681

phase change materials for transient thermal regulation [14].

The practicality of combining TEGs with PV cells in non-concentrated systems, however, has been called into question [15] as the introduction of the TEGs will act to increase the overall thermal resistance of the system, thus increasing the operating temperature of the PV cells, and reducing their efficiency. Meanwhile, the benefit provided by the TEGs is small, and does not compensate for the power loss of the PV cells, due to the low efficiency of TE materials [12].

When TEGs are integrated with concentrated photovoltaic (CPV) systems, however, many of the challenges associated with non-concentrated PV systems can be alleviated, allowing hybrid CPV-TEG systems to leverage several key advantages. CPV cells typically exhibit a lower temperature coefficient, making their performance less sensitive to the increase in operating temperature. The negative impact of the additional thermal resistance introduced by the TEG is therefore reduced, ensuring minimal performance degradation of the CPV cell due to temperature rise. Furthermore, the concentrated solar irradiance generates a larger temperature gradient across the TEG module, leading to a higher TE efficiency.

Theoretical studies have analysed the technical performance of hybrid CPV-TEG systems in recent years, particularly focused on power output and efficiency. Mahmoudinezhad et al. [16,17] studied a multi-junction hybrid CPV-TEG system numerically and experimentally, obtaining temperature and power output variations under transient operational conditions. The authors emphasised that the operational temperature imposed significant impact in the power generation efficiency of the hybrid system and needed to be controlled by optimizing both the optical concentration ratio (CR) and the convective heat transfer coefficient on the cold side.

Several studies have analysed the influence of the optical CR on the performance of hybrid CPV-TEG systems. Rejeb et al. [18] proposed an optimization model for CPV-TEG systems to maximize the system power output. The results indicated that increasing the optical CR had a positive effect on the energy conversion efficiency of the hybrid CPV-TEG system. Rezania and Rosendahl [19] reported similar results, showing that higher optical CR could significantly improve the power output of hybrid CPV-TEG systems, making it more preferrable than standalone CPV systems. However, Rodrigo et al. [20] investigated performance limits of hybrid CPV-TEG systems with triple-junction CPV cells, and reported that excessive solar CR negatively impacted the system performance due to thermal management challenges. Meanwhile, Singh et al. [21] identified that the maximum power output occurred at a specific optical CR under a solar irradiance of 1000 W/m^2. Yin et al. [22] further suggested that performance

This preprint research paper has not been peer reviewed. Electronic copy available at: https://ssrn.com/abstract=6589681

characteristics of CPV cells and TE material properties could significantly alter the effect of optical CR on power generation efficiency of hybrid CPV-TEG systems.

In addition to the optical CR, the benefits of maintaining a low temperature of the bottom surface of TEG modules have been investigated through the implementation of advanced cooling methods. Lekbir et al. [23] compared the overall power output of hybrid CPV-TEG systems with different cooling systems: natural air convection, nanofluid cooling, and the combination of both methods. The authors found that the power output of the hybrid CPV-TEG system with nanofluid cooling was the highest, and was 48% higher than that of the standalone CPV system. Gao et al. [24] explored the integration of PCM in hybrid CPV-TEG systems under non-uniform concentrated solar radiation. The study revealed that the PCM placement significantly influenced the temperature distribution of the system, with CPV temperature reduced by up to 19.22 K and system power output increased by 0.33 W. Rajaee et al. [25] utilized a combined cooling method of cobalt oxide (Co_3O_4) nanofluids and PCM heat sinks. Their findings indicated a 12% improvement in electrical efficiency compared to water-cooled systems, suggesting the benefits of hybrid cooling methods in hybrid CPV-TEG systems.

Previous research has demonstrated the feasibility of integrating TEGs with CPV systems to enhance the overall system efficiency. However, most of these studies are limited to specific coupling devices and system structures, making the results insufficient for guiding the design of hybrid CPV-TEG systems with alternative coupling configurations. In addition, although the interaction between the performance of the hybrid CPV-TEG system and operational conditions has been investigated, the results remain contradictory due to variations in the types of CPV cells and other parameters considered across studies. Furthermore, some studies have highlighted the influence of TE material properties, while there is still a lack of research incorporating advanced TE materials into hybrid CPV-TEG systems and systematically evaluating their impact. Existing literature offers few guidelines for selecting optimal TE materials under various operational scenarios, leaving a critical gap in practical implementation.

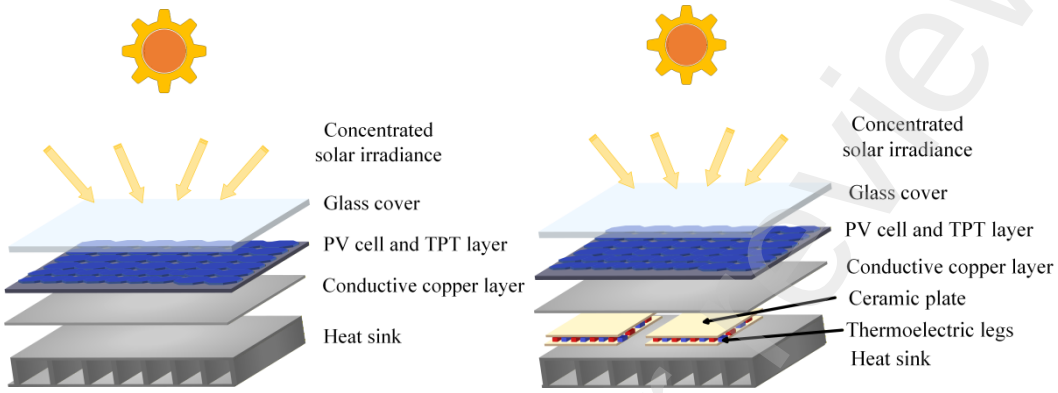
The present study addresses the research gaps identified above by simulating the performance of hybrid CPV-TEG systems along with comparison with standalone CPV systems. A detailed analysis is conducted to evaluate the influence of operational parameters, CPV performance characteristics, and TE material properties on system performance. In addition, a systematic material selection methodology is proposed and applied to evaluate and identify the most suitable TE materials for maximizing the efficiency of hybrid CPV-TEG systems. This study provides insights into the operational mechanisms, material optimization, and

This preprint research paper has not been peer reviewed. Electronic copy available at: https://ssrn.com/abstract=6589681

performance boundaries of hybrid CPV-TEG systems.

2. Modelling methodology

Figure 1 shows schematic diagrams of a standalone CPV system (Figure 1(a)), and the tandem hybrid CPV-TEG system proposed in this research (Figure 1(b)).



(a) (b)

Figure 1. Schematic diagrams of: (a) standalone CPV system, and (b) hybrid CPV-TEG system.

The standalone CPV system comprises a glass cover, a layer of single-junction GaAs solar cells with a tedlar-polyester-tedlar (TPT) back layer, a conductive copper layer, and a heat sink. The CPV-TEG system combines the standalone CPV system with a layer of TEG modules positioned between the copper layer and the heat sink. During operation, the incident sunlight over the PV module is absorbed by the PV cells for power generation, and the resulting waste heat is conducted to the top surface of the TEG layer. Simultaneously, the working fluid within the heat sink facilitates the cooling of the bottom surface of the TEG layer, thereby maintaining a temperature difference across the TEG modules. Through the Seeback effect, the temperature difference is used to generate electricity by the thermoelectric legs, contributing to the additional power output. The residual heat is then directed to the heat sink for dissipation.

In this research, a transient thermal model is developed to simulate the temperature distribution of the system with the assumptions described as follow:

i. The CPV and TEG are ideally insulated, so that the heat transfer from the system to the environment occurs only at the top and the bottom surfaces of the system. Consequently, heat is considered to flow only in one dimension.

ii. Since the temperature distribution through the thickness of each layer is approximately linear, the temperature at the middle point of the layer is chosen as a representative value for the temperature of the layer.

Preprint not peer reviewed

This preprint research paper has not been peer reviewed. Electronic copy available at: https://ssrn.com/abstract=6589681

iii. Packing factor of the CPV panel is 1, suggesting that the entire area of the CPV panel is effectively occupied by CPV cells.

iv. Ohmic losses are neglected in CPV cells.

v. Load resistance of each TEG module is equal to its internal resistance [4].

vi. Ambient temperature and incident solar irradiance without optical concentration are set to be 298.15 K and 1000 W/m^2 (refer to the standard AM 1.5G solar cell test condition).

vii. Wind speed constantly equals to 2.5 m/s [26].

Geometric parameters of each layer as well as the physical properties of the materials are listed in Table 1. To ensure high fidelity in the hybrid model, the TE material properties are treated as temperature-dependent variables. These properties are calculated dynamically within the simulation using second-order polynomial functions. The specific polynomial coefficients and the temperature ranges for which they are valid are detailed in Table S1 of the Supplementary Material.

Table 1. Geometric and material properties of hybrid CPV-TEG system [27–29].

Properties	**Unit**	**Glass cover (g)**	**TPT back layer (TPT)**	**Conductive layer (cl)**	**Ceramic plate (ce1 & ce2)**	**TE legs (te)**
Thickness	mm	3	0.3	0.3	0.2	1
Area	mm^2	40×40	40×40	40×40	10×10	0.15×0.15
Thermal conductivity	W·m^{-1}·K^{-1}	1.1	0.15	385	25	-
Absorptivity	-	0.05	-	-	-	-
Emissivity	-	0.92	-	-	-	-
Transmittance	-	0.94	-	-	-	-

2.1 Energy balance model and governing equations

The electro-thermal performance of the CPV panel is captured through a series of coupled energy balances that account for conductive, convective, and radiative heat exchanges. To maintain focus on the primary system-level interactions, the detailed layer-by-layer energy conservation equations for the glass cover, TPT back layer, and copper conductive layer are provided in

Preprint not peer reviewed

This preprint research paper has not been peer reviewed. Electronic copy available at: https://ssrn.com/abstract=6589681

Section S1 of the Supplementary Material. These equations utilize standard 1-D steady-state heat transfer principles and empirical correlations for convective heat flux.

The critical thermal-electrical coupling within the system is defined at the CPV cell layer. The energy balance for the CPV cell accounts for the incident concentrated solar irradiance, CPV electrical power generation, convective and radiative heat loss, and the resulting waste heat conducted to the TEG layers:

$$CG\left(\alpha_{\mathrm{g}}+\alpha_{\mathrm{pv}}\tau_{\mathrm{g}}\right)=\dot{P}_{\mathrm{pv}}+\dot{Q}_{\text{pv-TEG}}+\dot{Q}_{\mathrm{conv}}+\dot{Q}_{\mathrm{rad}} \tag{1}$$

where CG denotes the product of the optical CR and solar irradiance, α is the absorptivity of the layer, and $\dot{Q}_{\text{g-pv}}$ is the net thermal flux from the glass to the CPV cells, with subscripts 'g', 'pv', and 'TEG' referring to the glass cover, the CPV cells, and the TEG layers. Furthermore, $\dot{Q}_{\mathrm{rad}}$ and $\dot{Q}_{\mathrm{conv}}$ are the radiative and convective heat fluxes on the top surface of the glass cover, with further details provided in Supplementary Material.

The electrical power output per unit area ($\dot{P}_{\mathrm{pv}}$) is strongly dependent on the cell's operating temperature (T_{pv}), calculated as [27]:

$$\dot{P}_{\mathrm{pv}}=\eta_{\mathrm{ref}}\left[1-\beta\left(T_{\mathrm{pv}}-T_{\mathrm{ref}}\right)\right]CG\alpha_{\mathrm{pv}}\tau_{\mathrm{g}} \tag{2}$$

where η_{ref} is the reference conversion efficiency of the solar panel at the standard test condition of temperature T_{ref}, which is normally 25 °C or 298.15 K, and β is the temperature coefficient of the solar panel as provided by the manufacturer; see Table 3 for values used in this work.

The TEG sub-system consists of n pairs of thermoelectric legs integrated between two ceramic plates, positioned between the CPV's conductive copper layer and the heat sink. The thermal distribution within the TEG module is governed by steady-state energy balances for the ceramic plates and the thermoelectric legs, which is documented in Section S1.2 of the Supplementary Material.

The power generation of the TE legs ($\dot{P}_{\mathrm{te}}$) is driven by the Seebeck effect across the temperature gradient between the hot and cold junctions:

$$\dot{P}_{\mathrm{te}}=S\Delta TI-R_{\mathrm{in}}I^{2}=R_{\mathrm{L}}I^{2}=\frac{R_{\mathrm{L}}\left(S\cdot\Delta T\right)^{2}}{\left(R_{\mathrm{in}}+R_{\mathrm{L}}\right)^{2}} \tag{3}$$

where S represents the Seebeck coefficient of the TE material (from Table S1), ΔT represents the temperature difference between the hot side and cold side of the TE legs, R_{in} is the internal

Preprint not peer reviewed

This preprint research paper has not been peer reviewed. Electronic copy available at: https://ssrn.com/abstract=6589681

electrical resistance, R_L represents the external load resistance, and I represents the load current.

The power generation efficiency of the TEG module, η_{te}, is defined as:

$$\eta_{te} = \frac{\dot{P}_{te}}{\dot{Q}_{ce1\text{-}te}} \tag{4}$$

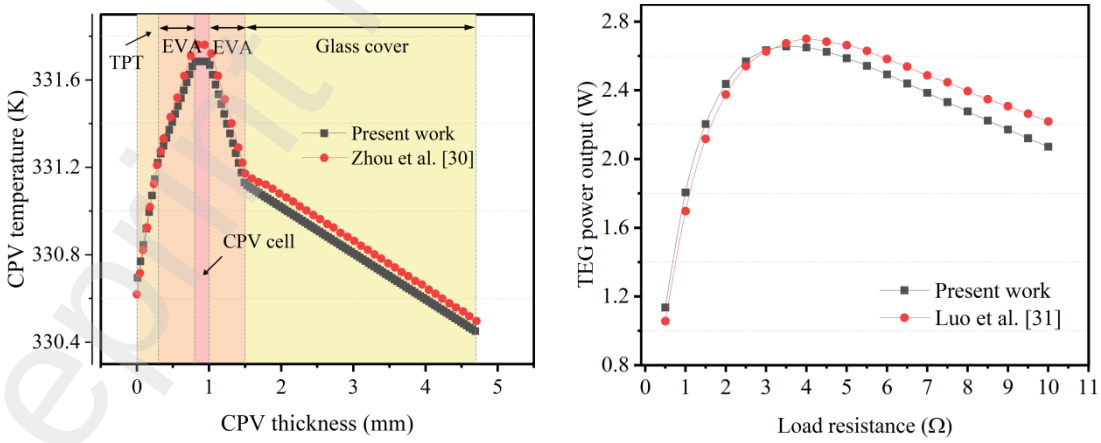
To evaluate the overall benefit of the hybrid configuration, the total system efficiency (η_{sys}) is defined as the summation of the individual efficiencies of the CPV and TEG components:

$$\eta_{sys} = \frac{\dot{P}_{pv} + \dot{P}_{te}}{CG} \tag{5}$$

This integrated metric serves as the primary criterion for determining the performance boundaries of the hybrid CPV-TEG system relative to the standalone CPV configuration.

2.2 Model validation

In order to validate the models presented above, numerical prediction by the models are compared with data from previous research. The CPV model in the present work is validated by comparison with the 3-D finite element method described by Zhou et al. [30] under the same operational conditions. A comparison of the temperature profile through the CPV panel layers is shown in Figure 2(a). It can be seen that the results are in good agreement with a maximum temperature difference of 0.077 K. Similarly, TEG model predictions are compared with the experimental data reported by Luo et al. [31]. The power output of a TEG module for various load resistances is plotted in Figure 2(b). Similar as above, acceptable agreement is observed between the TEG model and the data, with an average error of 3.9%.

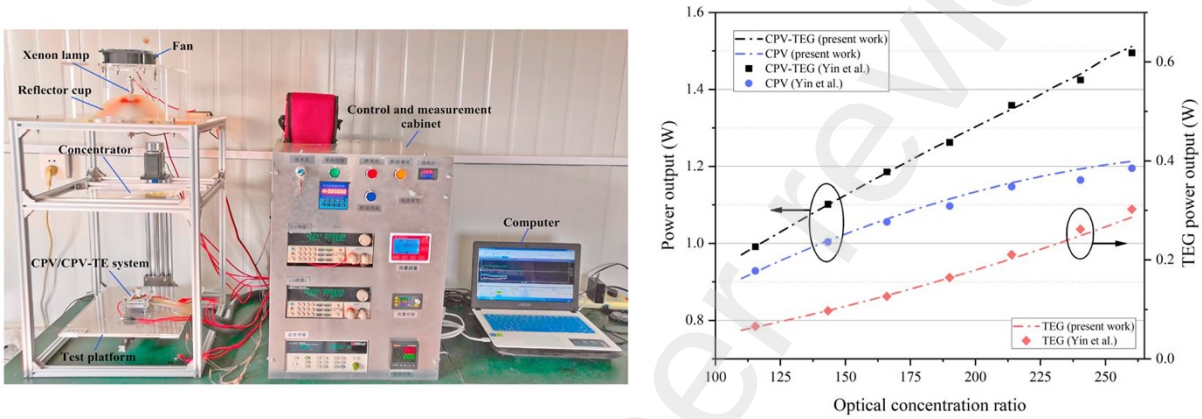


(a) (b)

Figure 2. (a) Temperature distribution validation of the CPV model, and (b) power output validation of the TEG model.

This preprint research paper has not been peer reviewed. Electronic copy available at: https://ssrn.com/abstract=6589681

Simulation of the hybrid CPV-TEG system requires coupling the two separate sub-system models described above, and further validation has been performed of the coupled model using experimental data provided by Yin et al. [22]. The experimental apparatus and a comparison of results are shown in Figure 3. According to the results, the average errors for the total CPV-TEG power output, PV power output, and TEG power output are 0.8%, 1.2%, and 2.9%, respectively. On the basis of these and the observations above for the sub-system models, the proposed model is deemed to have sufficient accuracy for the exploratory purposes of our study.



(a) (b)

Figure 3. (a) Experimental apparatus of Yin et al. [22] from which data was taken for validation, and (b) validation of power output predictions from the CPV-TEG model against the data.

3. Results and discussion

A comparative analysis is conducted to explore the performance of the proposed hybrid CPV-TEG system relative the standalone CPV system. The optical CR and the cold-side convective heat transfer coefficient, which have been highlighted in previous studies as key factors influencing hybrid CPV-TEG system performance [22,32,33], are of particular interest here. Additionally, the key performance characteristics of different CPV cell types, such as the reference efficiency and the temperature coefficient, are also considered, as the integration of TEGs may yield varying benefits depending on the specific cell technology employed. In what follows, the effect of the optical CR is discussed in Section 3.1, and that of the cold-side convective heat transfer coefficient in Section 3.2; in both cases results are shown for the three common types of CPV cells listed in Table 2. A detailed analysis aimed at comprehensively evaluating the influence of selected CPV cell on the overall efficiency and power generation of the combined CPV-TEG system, is presented in Section 3.3.

Preprint not peer reviewed

This preprint research paper has not been peer reviewed. Electronic copy available at: https://ssrn.com/abstract=6589681

Table 2. Characteristics of three common CPV cell technologies [19,32,34].

Type of CPV cells	Typical concentration ratio	Reference efficiency	Temperature coefficient
Polycrystalline Si	Low (< 20)	17.0%	0.00451/K
Monocrystalline Si	Medium (20 – 100)	21.2%	0.00270/K
Triple-junction GaInP/ GaInAs/Ge	High (> 100)	40.8%	0.00047/K

3.1 Effect of optical concentration ratio

In this section, the performance of both the hybrid CPV-TEG system and the standalone CPV system are analysed under various optical CRs. The three selected CPV cells, whose characteristics are given in Table 2, are simulated under their respective typical working CRs. The convective coefficient (h_w) at the cold side of the TEG is set to 5000 W/m^{2}K, as this value provide sufficient cooling capacity and mitigate its impact on the system performance.

Figure 4 present the power output, system efficiency, and cell temperature of the hybrid CPV-TEG system with the three types CPV cells under varying optical CRs. The results in Figure 4 (a)-(d) indicate that the inclusion of the TEG modules cannot improve the overall system efficiency when integrating with either polycrystalline silicon (poly-Si) or monocrystalline silicon (mono-Si) CPV cells. At low CRs, the power output of the standalone CPV system and the hybrid CPV-TEG system are approximately equal. However, as the CR increases, the standalone system begins to slightly outperform the hybrid system. Specifically, for the mono-Si cell, the standalone system attains an 0.5 W higher output power than the hybrid system at CR = 100. It is noted that, in both cases, the loss in overall performance arises from the increased cell temperature in the hybrid system, that leads to a CPV efficiency deterioration that far outweighs the slight added generation from the TEG.

Considering the loss in overall performance along with the additional technical complexity and costs associated with the hybrid system, such TEG module integration is not deemed feasible.

Preprint not peer reviewed

This preprint research paper has not been peer reviewed. Electronic copy available at: https://ssrn.com/abstract=6589681

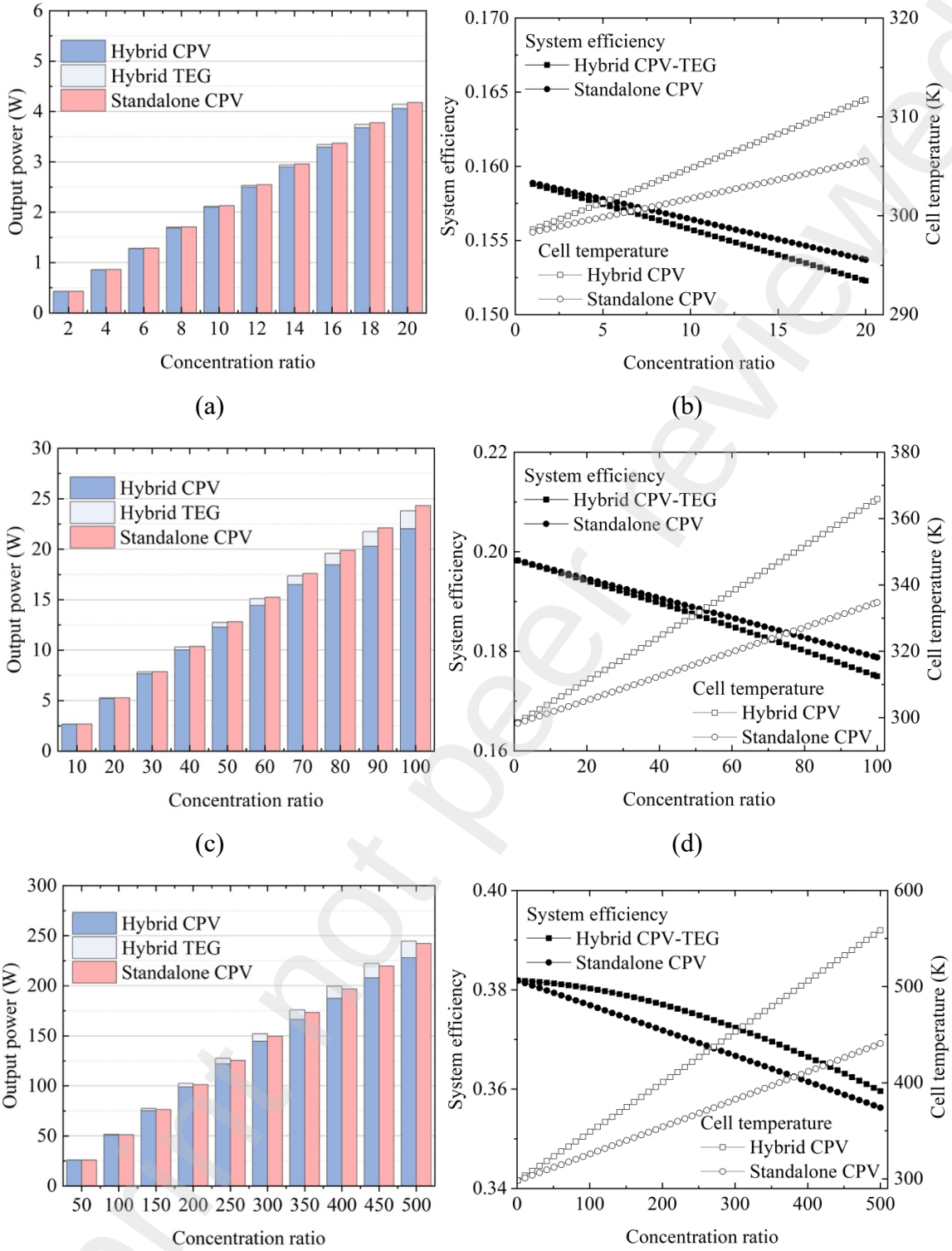


Figure 4. Power output, system efficiency and cell temperature of hybrid CPV-TEG and standalone CPV systems with (a)-(b) poly-Si cell, (c)-(d) mono-Si cell, and (e)-(f) triple-junction CPV cell.

On the other hand, the integration of TEG modules with a triple-junction CPV cell can lead to an improvement in system performance, as shown in Figure 4(e)-(f). At a CR of 50, the

This preprint research paper has not been peer reviewed. Electronic copy available at: https://ssrn.com/abstract=6589681

power outputs and efficiencies of the standalone and hybrid systems are approximately equal, both reaching 26 W (38% efficiency). However, the power output of the hybrid system increases more rapidly as the CR increases. Figure 4(e)-(f) shows that the performance advantage of the hybrid system becomes more pronounced as the CR increases to 200-300, reaching a maximum difference of 2.3 W, and that this advantage diminishes as the CR further increases to 500.

For all three types of cells, the performance of the hybrid system follows a similar trend, with any potential benefit eventually decreasing at higher CR values. For poly-Si and mono-Si cells, the integration with TEG modules yields no additional efficiency improvement at any CR level, whereas for the triple-junction cell, the hybrid system outperforms the standalone CPV system within the studied CR range by up to 2.3 W, although this potential benefit vanishes at very high CR. In all cases, these trends can be attributed to the temperature-induced performance degradation of the cells. The integration of TEG modules introduces additional thermal resistance between the CPV system and the heat sink, leading to higher cell temperatures in the hybrid CPV-TEG system compared to the standalone CPV system. This temperature increase reduces the CPV sub-system power output, and this effect becomes more significant as the optical CR increases.

3.2 Effect of cold-side convective heat transfer coefficient

In addition to the optical CR, the cooling method is another critical factor influencing the performance of hybrid CPV-TEG systems. A higher cold-side convective heat transfer coefficient mitigates the CPV cell temperature increase, thereby alleviating the temperature-induced power losses. On the other hand, improved cooling enhances the power output of the TEG modules by increasing the temperature difference across the TE legs while maintaining a relatively low TEG operating temperature.

It is noteworthy that the studied ranges of the cold-side convective heat transfer coefficient are set to be different for the three types of CPV cells due to their typical CR. For each type of cell, simulations were conducted at three levels of optical CR, with corresponding ranges of the cold-side convective coefficient. The simulation results, presented in Figure 5, confirm that increasing the cold-side convective coefficient has a positive effect on the performance of both the hybrid CPV-TEG and standalone CPV systems. However, when the optical CR is below 100, the power output of the hybrid CPV-TEG system does not surpass the standalone CPV system, even when the cold-side convective coefficient increases to 10000 W/m^2K. At a CR of

This preprint research paper has not been peer reviewed. Electronic copy available at: https://ssrn.com/abstract=6589681

300, the overall efficiency of the hybrid CPV-TEG system, utilising a triple-junction CPV cell, surpasses that of the standalone CPV system when the cold-side convective coefficient is higher than 2000 W/m^{2}K. When the CR is further increased to 500, achieving the performance advantage of the hybrid CPV-TEG system requires more advanced cooling methods, with the cold-side convective heat transfer coefficient above 4500 W/m^{2}K.

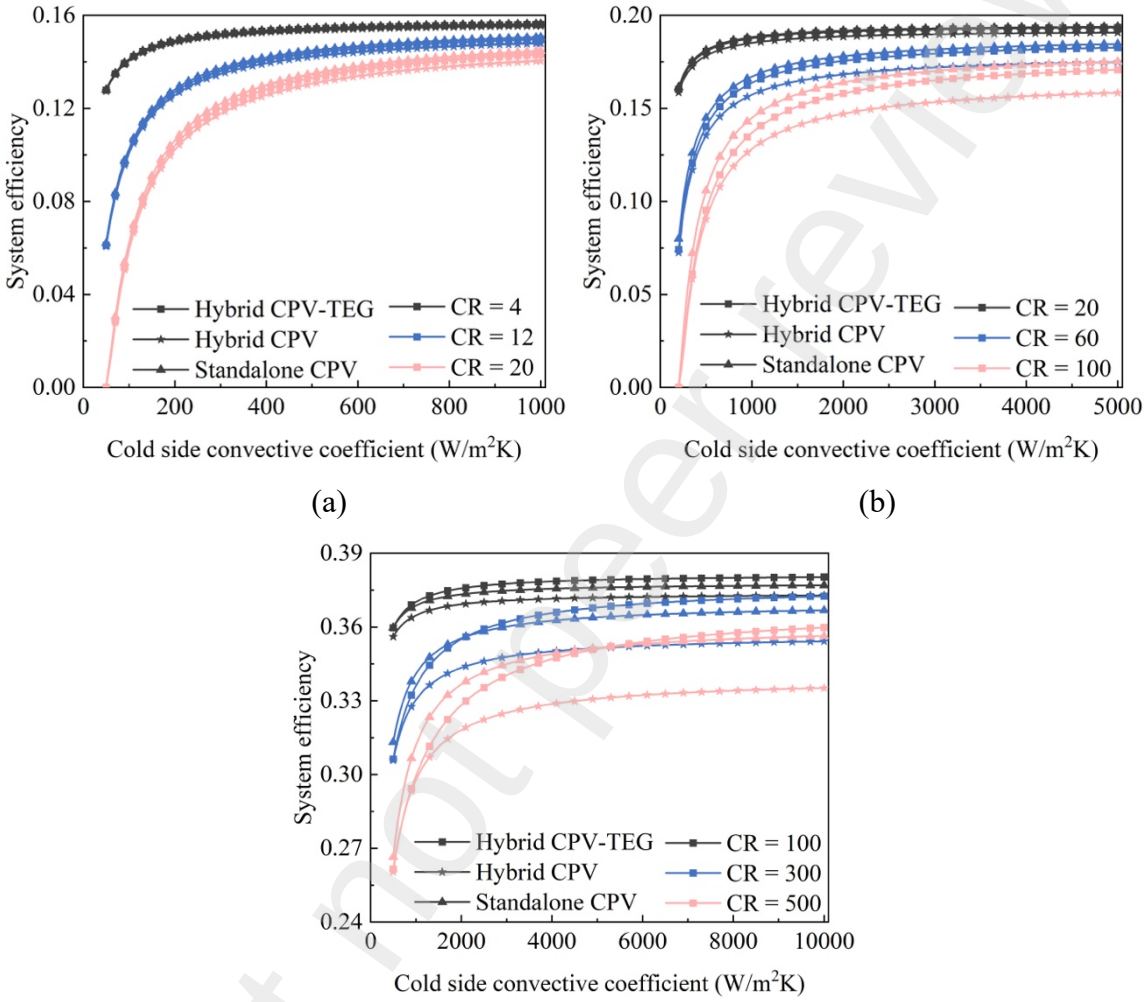


Figure 5. Hybrid CPV-TEG and standalone CPV system efficiency variations with cold-side convective heat transfer coefficient and for: (a) poly-Si CPV cell, (b) mono-Si CPV cell, and (c) triple-junction CPV cell cases.

3.3 Effect of CPV cell performance

As mentioned in previous sections, the performance of the hybrid CPV-TEG system is primarily influenced by the characteristics of the CPV cell, particularly the reference efficiency (η_{ref}) and the temperature coefficient (β). In this section, the effects of these two performance parameters on the system efficiency of the hybrid CPV-TEG system are analysed for three

This preprint research paper has not been peer reviewed. Electronic copy available at: https://ssrn.com/abstract=6589681

optical CRs, i.e., 20 (low to medium), 100 (medium to high), and 500 (high to ultra-high). The cold-side convective heat transfer coefficient is set to 5000 W/m^2K to provide sufficient cooling capacity and mitigate its impact on the system performance.

Figure 6 shows the efficiency of the hybrid and standalone CPV systems, with results coving a range of temperature coefficients and reference efficiencies. As shown in Figure 6, a small temperature coefficient leads to insignificant variation on the performance of the hybrid CPV-TEG system when CR = 20. However, the temperature coefficient plays an important role when the system is operated under high optical CRs and, thus, temperatures. A low temperature coefficient increases the hybrid overall system efficiency and allows this outperform the standalone CPV system, as shown in Figure 6. When $\eta_{ref} = 10\%$ and $\beta = 0.0005/K$, the hybrid system has an efficiency of 10%, which represents a 24% improvement over the standalone system at a CR of 500. The results also suggest that TEG integration is advantageous for CPV systems with comparatively low reference efficiency. Conversely, for higher reference cell efficiencies, the standalone CPV system tends to have a higher power output and efficiency, supressing the relative contribution of the TEG modules.

Preprint not peer reviewed

This preprint research paper has not been peer reviewed. Electronic copy available at: https://ssrn.com/abstract=6589681

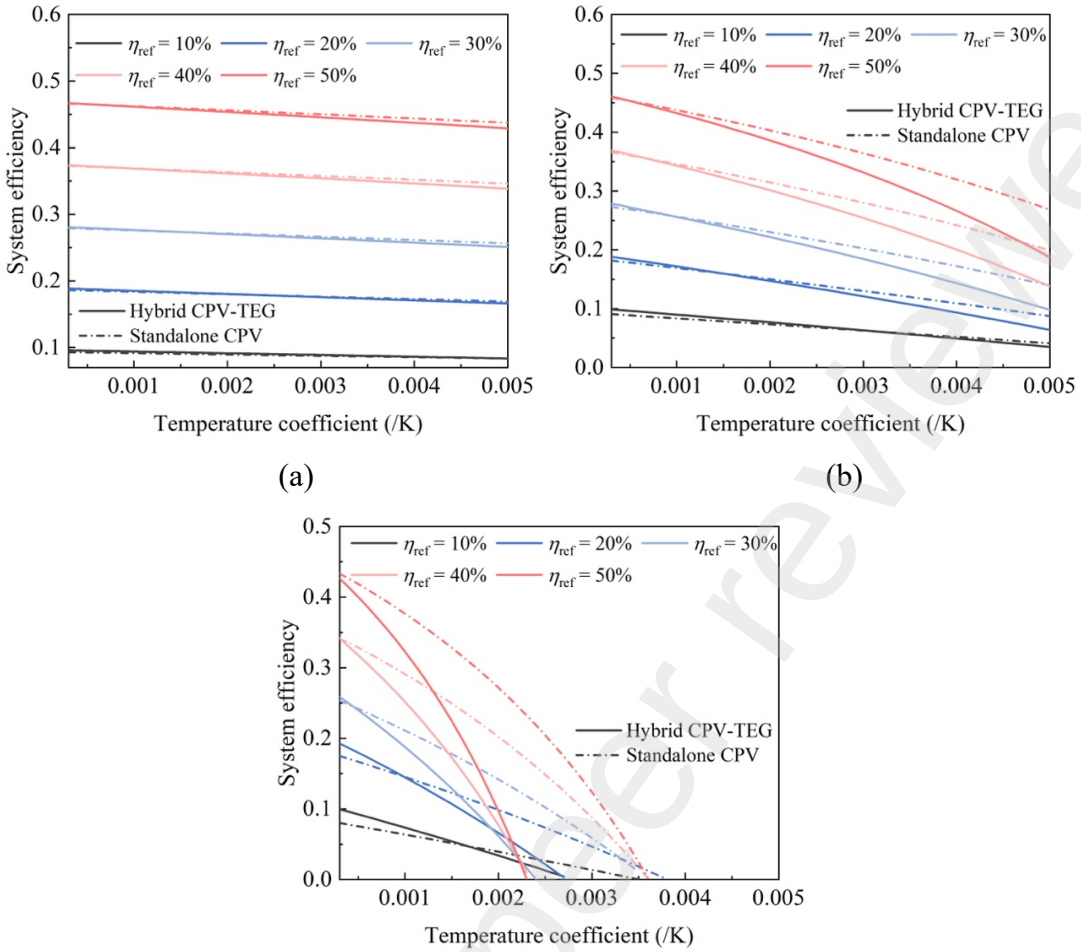


Figure 6. System efficiency variations with temperature coefficient for various CPV reference efficiencies and for: (a) CR = 20, (b) CR = 100, and (c) CR = 500.

3.4 Effect of thermoelectric material properties

The hybrid CPV-TEG system efficiency for different TE Seebeck coefficient (α), thermal conductivity (κ), and electrical resistivity (ρ) values is presented in Figure 7. The cell performance characteristics are set to match the baseline values of the triple-junction cell, as stated in Table 2. The values of the TE material properties are normalized with respect to the baseline values summarised in Table S1, and are varied from -50% to +50% of these values. Since the impact of any single TE material property can be influenced by the other two properties, when one of the three TE material properties is varied within the considered range, the other two properties are held at three distinct levels: -50% of the baseline value, the baseline value, and +50% of the baseline value. By analysing the simulation results, the interacted effects and the relative importance of each pair of TE material properties can be identified and evaluated.

This preprint research paper has not been peer reviewed. Electronic copy available at: https://ssrn.com/abstract=6589681

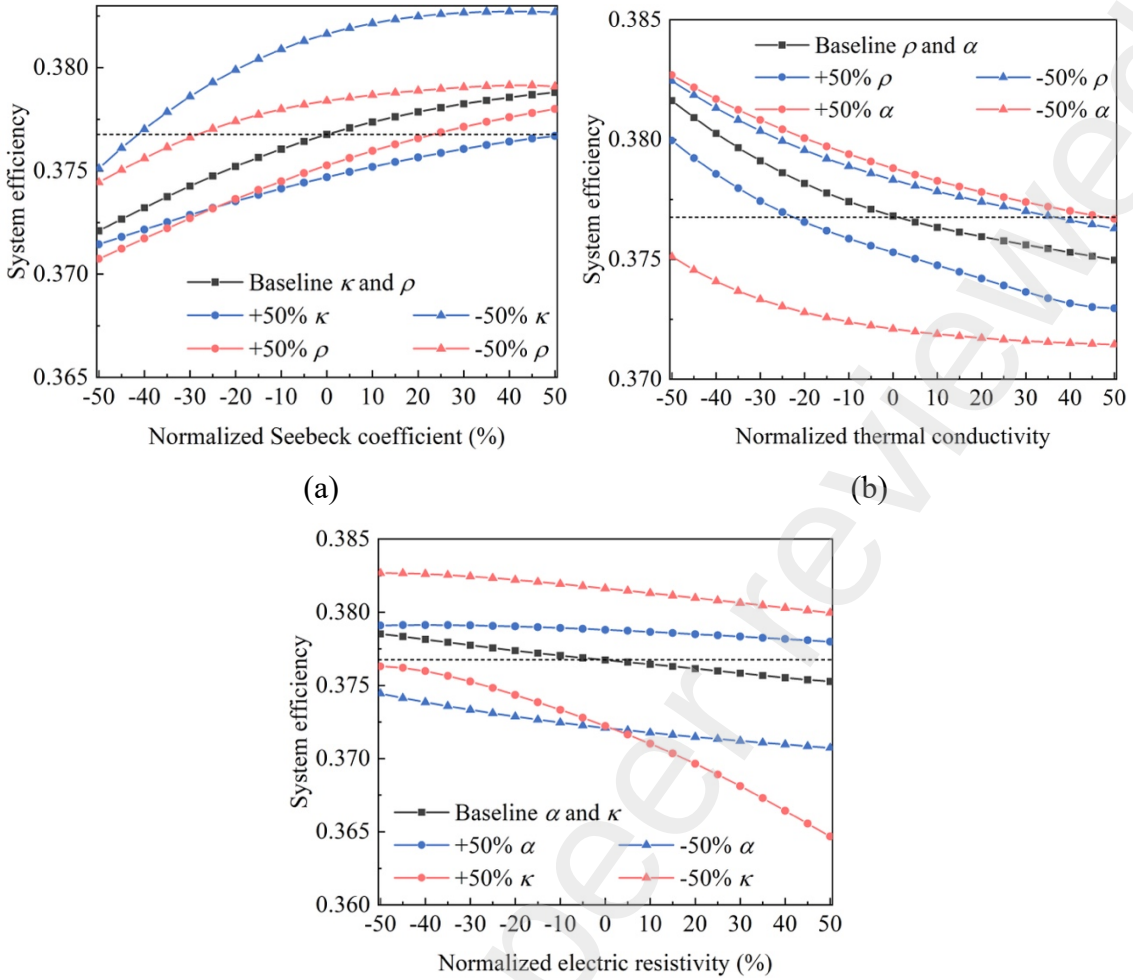


Figure 7. System efficiency variation with normalized: (a) TE Seebeck coefficient, (b) TE thermal conductivity, and (c) TE resistivity changes when CR = 300, h_w = 2000 W/m^{2}K.

According to Figure 7, an increase in α is preferred as it improves the TEG efficiency and subsequently mitigates the efficiency drop of the CPV cells. This is because the heat from the bottom surface of the CPV panel is more effectively converted into electrical power. When the change of α reaches +50%, the efficiency of the hybrid CPV-TEG system reaches 37.8%, provided the other two properties remain unchanged at their baseline values. However, the benefit brought by increasing α is reduced when either κ or ρ are also increased by 50%. Specifically, when κ increases by 50%, the system efficiency remains at 37.7%, which is the same as the baseline scenario, indicating that the opposing effects of increasing both α and κ counteract each other. On the other hand, when ρ increases by 50%, the system efficiency remains higher than the baseline, suggesting that the influence of α dominates that of ρ.

A preference for smaller κ is indicated in Figure 7. Compared to the baseline values, a lower κ enhances the TEG efficiency by creating a larger temperature gradient across the TE legs due to

Preprint not peer reviewed

This preprint research paper has not been peer reviewed. Electronic copy available at: https://ssrn.com/abstract=6589681

reduced heat conduction ability. When κ decreases by 50% and the other two properties remain unchanged, the efficiency of the hybrid CPV-TEG system reaches 38.2%. Nevertheless, the benefit of a 50% reduction in κ is completely negated when α simultaneously decreases by 50%, reducing the system efficiency to 37.5% which is 0.5% lower than the baseline. Meanwhile, the influence of κ still outweighs the influence of ρ, further indicating the importance of κ.

When considering ρ, the efficiency of the hybrid CPV-TEG system improves as ρ decreases, because it suppresses the Ohmic losses in TEG modules, thereby enhancing the efficiency of TEG modules. As shown in Figure 7, when ρ decreases by 50%, the system efficiency reaches 37.8%. However, ρ has the least significant impact on the system efficiency among all the TE material properties. The change caused by variations in ρ can be offset by adjustments to the other two properties, reinforcing its relatively minor role in influencing the overall system performance.

3.5 Thermoelectric material selection by multi-criteria decision making

While the performance of standalone TEG modules can be assessed with simple parameters like the figure of merit and power factor, integrating them with CPV cells introduces additional considerations. As discussed in the previous sections, the temperature difference needed for high TEG efficiency may lead to thermal degradation of CPV power generation efficiency and aging acceleration. Furthermore, if economic factors need to be considered in the future for commercial application, it will add another layer of complexity and trade-offs into the decision-making process. In order to address this challenge, a systematic material selection methodology is necessary.

Multi-criteria decision making (MCDM) is a useful framework for identifying optimal candidates from a set of alternatives. In designing a hybrid CPV-TEG system, TE material selection must account for three critical aspects: (a) intrinsic TE material properties, (b) system-level objectives such as maximizing energy conversion efficiency and minimizing heat loss), and (c) practical constraints such as cost, manufacturability, and engineering preferences. To address these multifaceted requirements, the analytical hierarchy process (AHP) provides a hierarchical structure to systematically integrate quantitative performance metrics with qualitative criteria, and assign a relative weight to each attribute. After the determination of relative weights via AHP, the technique for order preference by similarity to ideal solution (TOPSIS) method is employed to objectively evaluate candidate materials. TOPSIS quantifies the distance of each material to an "ideal" solution (optimal performance across all attributes) and its distance from a "negative ideal" solution (worst-case performance), enabling a data-driven ranking. The full mathematical framework for these methods, including the normalization and closeness coefficient derivations

This preprint research paper has not been peer reviewed. Electronic copy available at: https://ssrn.com/abstract=6589681

(Eqs. S17–S27), is provided in Section S2 of the Supplementary Material.

In this study, the relative importance between three TE material properties are assigned according to the results discussed in Section 3.4, and the calculated relative weights of each property are summarised in Table 3. Several bismuth-telluride-based TE materials with diverse properties reported in the previous literatures [21,35–44] and the final rankings by AHP -TOPSIS framework are listed in Table 4.

Table 3. Relative importance of three TE material properties.

	α	κ	ρ
α	1	1	3
κ	1	1	2
ρ	0.33	0.5	1
W	0.4434	0.3874	0.1692

Table 4. Ranking of selected TE materials [21,35–44].

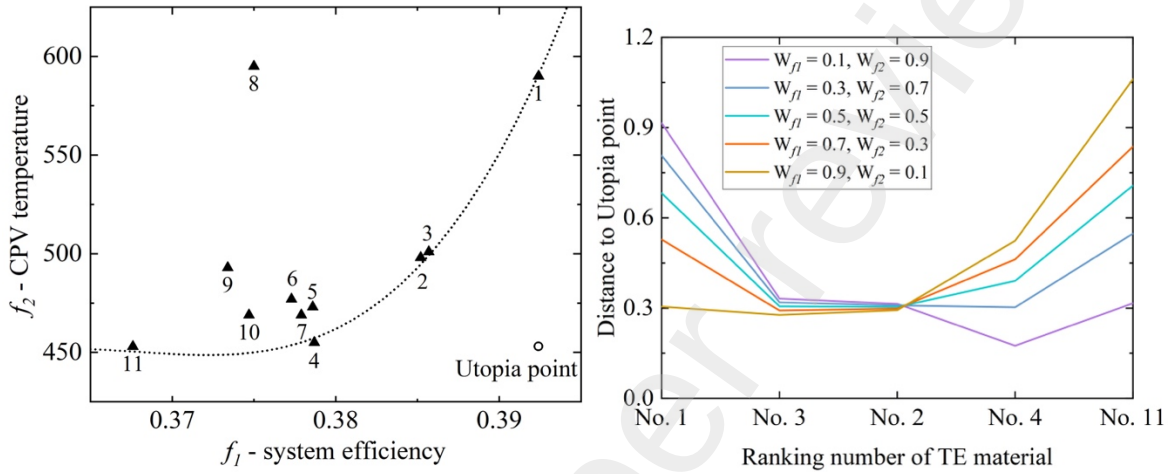
Material	α **(×10^{-6} V/m)**	κ **(W/mK)**	ρ **(×10^{-5} Ωm)**	**Ranking**
Porous $Bi_{2.0}Te_{2.7}Se_{0.3}$	210	0.24	3.90	1
7.5 wt.% Ag-Bi_2Te_3	125	0.46	0.67	2
$Bi_{0.5}Sb_{1.5}Te_3$ via liquid phase sintering	200	0.60	2.15	3
Bi_2Te_3–single wall carbon nanotube	160	0.6	1.81	4
15 wt.% $CaSiO_3$-Bi_2Te_3	220	0.35	7.69	5
8 mol % $FeTe_2$-$Bi_{0.4}Sb_{1.6}Te_3$	220	0.97	1.25	6
$Y_{0.25}Bi_{1.75}Te_3$	150	0.85	0.87	7
$Cu_{0.87}Bi_2Te_{2.69}$	120	0.8	1.16	8
$Bi_{1.95}Ge_{0.05}Te_3$	200	1.05	1.95	9
Bi_2Te_3 via liquid state manipulation	125	1.4	0.77	10

While the AHP-TOPSIS framework ranks TE materials based on the values across individual material properties, it does not inherently verify whether the collective interaction of these properties translates to optimal system-level performance in the hybrid CPV-TEG system. Therefore, Ashby's objective functions are integrated into the evaluation process. The selected

Preprint not peer reviewed

This preprint research paper has not been peer reviewed. Electronic copy available at: https://ssrn.com/abstract=6589681

objective functions represent system-specific performance targets and validate whether the top-ranked materials from AHP-TOPSIS framework align with the hybrid CPV-TEG system's operational objectives. In this study, two critical performance objectives are defined for the hybrid CPV-TEG system: (1) maximizing overall system efficiency (f_1), which quantifies the combined energy conversion effectiveness of the CPV and TEG modules, and (2) minimizing the operating temperature of the CPV cell (f_2) to mitigate thermal degradation and ensure long-term stability.



(a) (b)

Figure 8. (a) Performance assessment of TE materials and (b) sensitivity analysis of distances to Utopia point with varying weights.

The performance of TE materials is evaluated in the objective space as illustrated in Figure 8. A Pareto-efficient frontier is established, highlighting non-dominated candidates (nos. 1–4) and extreme performer (no. 11), while materials nos. 5–10 are classified as dominated solutions due to inferior performance in both criteria. Notably, the top-ranked materials from the AHP-TOPSIS framework align with the Pareto set, validating the effectiveness of the material selection methodology.

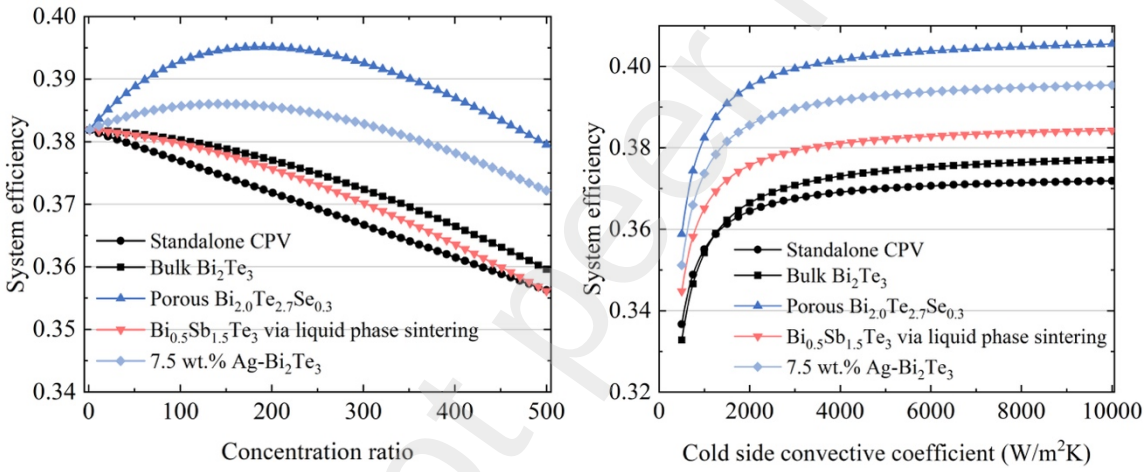
To quantitatively assess performance, a Utopia point is defined, representing the theoretical optimal values of normalized f_1 and f_2. The normalization and Euclidian distance (D_i) of each material to the Utopia point is calculated from:

$$f_{normal} = \frac{f - f_{min}}{f_{max} - f_{min}} \tag{6}$$

This preprint research paper has not been peer reviewed. Electronic copy available at: https://ssrn.com/abstract=6589681

$$D_i = \sqrt{W_{f_1} \cdot \left(1 - f_{1i,normal}\right)^2 + W_{f_2} \cdot f_{2i,normal}^2} \quad (7)$$

where W_{f1} and W_{f2} reflect the weights of objective functions. A systematic variation of weights W_{f1} and W_{f2} reveals the adaptability of material rankings to design priorities, as shown in Figure 8(b). Under balanced weighting conditions ($W_{f1} = W_{f2} = 0.5$), material no. 2 and no. 3 demonstrate optimal equilibrium, achieving competitive system efficiency levels while maintaining low CPV temperatures, highlighting their suitability for scenarios requiring moderate prioritization of both objectives. When the weighting scheme shifts toward system efficiency ($W_{f1} > 0.5$), the priority of material No. 1 improves due to its superior Seebeck coefficient and hence system efficiency. Conversely, prioritizing CPV temperature control ($W_{f2} > 0.5$) reveals the strength of material no. 4, corresponding to its high thermal conductivity favoured by the CPV cell.



(a) (b)

Figure 9. Hybrid CPV-TEG system performance (system efficiency) comparisons with various TE materials for different: (a) optical CRs, and (b) cold-side convective coefficients.

Figure 9 shows the performance of hybrid CPV-TEG systems utilizing the top three TE materials identified through the proposed selection methodology against the standalone CPV system and the baseline hybrid CPV-TEG system. As depicted in Figure 9, the material selection methodology successfully identifies TE materials with superior performance metrics that contribute to hybrid system efficiency. The best-performing TE material (porous $Bi_{2.0}Te_{2.7}Se_{0.3}$) achieves a peak system efficiency of 40%. The second-best material also enhances system efficiency across all optical CRs, further validating the robustness of the selection process. Even though the third-best TE material ($Bi_{0.5}Sb_{1.5}Te_3$ via liquid phase sintering) shows a faster decline in system efficiency than the baseline hybrid CPV-TEG system when the CR increases, it still

This preprint research paper has not been peer reviewed. Electronic copy available at: https://ssrn.com/abstract=6589681

performs moderately better than the standalone CPV system. Figure 9 further reinforces the effectiveness of the material selection methodology by demonstrating that the top three TE materials consistently achieve higher system efficiencies across a range of cold-side convective heat transfer coefficients, with the best-performing TE material peaking at 41%.

4. Conclusions

In this study, the performance of hybrid CPV-TEG systems was simulated using a detailed thermal model, and results were compared to those of standalone CPV systems. An in-depth analysis of operational parameters, cell performance characteristics, and TE material properties was conducted to investigate their influence on system performance. Based on the performance analysis, a systematic material selection methodology, combining AHP and TOPSIS, was implemented to identify the suitable TE materials for integration with CPV systems.

The simulation results reveal that the efficiency of hybrid CPV-TEG systems strongly depends on the interplay between the concentration ratio and cooling performance. For typical cooling fluxes, benefits relative to standalone CPV systems are only possible at intermediate CRs and when using triple-junction cells. A performance advantage of hybrid systems is observed when sufficient thermal management is applied, particularly at medium to high optical CRs. At a CR of 300, the system demonstrates superior performance when the cold-side convective heat transfer coefficient exceeds 2000 W/m²K. At higher CRs, e.g., 500, the required cooling performance increases, with optimal operation observed when the heat transfer coefficient exceeds 4500 W/m²K. The findings underscore the need for tailored cooling designs to realize the full potential of hybrid CPV-TEG systems, particularly at high concentration levels. Additionally, these results provide practical benchmarks for system design. For example, with moderate CRs, conventional cooling strategies may suffice, whereas high-concentration systems necessitate enhanced convective or advanced active cooling techniques.

The findings also highlight that the integration of TEG modules is particularly beneficial for CPV systems with low reference efficiency (η_{ref}) and low temperature coefficients (β), especially at high optical CRs. At a CR of 500, a hybrid CPV-TEG system employing cells with η_{ref} = 10% and β = 0.0005 achieves a system efficiency of 10%, representing a 24% improvement over the standalone CPV system. Conversely, CPV cells with higher reference efficiency produce sufficient power output on their own, reducing the relative contribution of the TEG modules to overall system generation.

In an effort to evaluate and rank TE materials systematically, the relative importance matrix,

This preprint research paper has not been peer reviewed. Electronic copy available at: https://ssrn.com/abstract=6589681

derived by pairwise comparisons of critical TE material properties, is used as input for the AHP method. The results of the material selection methodology validate its robustness and effectiveness. The top three TE materials identified consistently outperform both the standalone CPV system and the baseline hybrid CPV-TEG system, with the best-performing TE material achieving a peak system efficiency of 41%.

In summary, the CPV-TEG system achieves optimal performance under the following conditions:

1. Integration of CPV cells with low temperature coefficients (β).
2. Implementation of high-performance TE materials, identified through a robust AHP-TOPSIS framework.
3. Operation at high optical CRs with effective thermal management, particularly cold-side heat transfer enhancements.

This study provides a systematic approach to improve the performance advantage of hybrid CPV-TEG systems, offering clear guidelines for CPV cell selection, TE material evaluation, and thermal management design. Future research should focus on the development of TE materials with higher figure-of-merit, as well as advanced cooling technologies to further enhance the performance of the hybrid system under ultra-high optical concentration conditions.

Acknowledgments

This work was supported by Shenzhen Science and Technology Innovation Commission (KCXFZ20211020165004006, KCXST20221021111609024, KCXFZ20240903093459001). Data supporting this publication can be obtained on request from cep-lab@imperial.ac.uk. For the purpose of Open Access, the authors have applied a CC BY public copyright license to any Author Accepted Manuscript version arising from this submission.

Preprint not peer reviewed

This preprint research paper has not been peer reviewed. Electronic copy available at: https://ssrn.com/abstract=6589681

519 **References**

520 [1] International Energy Agency. Global Energy Review 2021: Assessing the effects of
521 economic recoveries on global energy demand and CO_2 emissions in 2021. 2021.

522 [2] Venkateswari R, Sreejith S. Factors influencing the efficiency of photovoltaic system.
523 Renew Sustain Energy Rev 2019;101:376–94.
524 https://doi.org/10.1016/j.rser.2018.11.012.

525 [3] Rana S, Date A, Akbarzadeh A. Solid-state devices. In: Markides CN, Wang K, editors.
526 Power generation technologies for low-temperature and distributed heat, Woodhead
527 Publishing; 2023. https://doi.org/10.1016/C2018-0-03181-3.

528 [4] Ji D, Hu S, Feng Y, Qin J, Yin Z, Romagnoli A, et al. Geometry optimization of solar
529 thermoelectric generator under different operating conditions via Taguchi method.
530 Energy Convers Manag 2021;238:114158.
531 https://doi.org/10.1016/j.enconman.2021.114158.

532 [5] Vining, C. An inconvenient truth about thermoelectrics. Nat Mater 2009;8:83–85.
533 https://doi.org/10.1038/nmat2361.

534 [6] Markides, CN. Low-concentration solar-power systems based on organic Rankine
535 cycles for distributed-scale applications: overview and further developments. Front
536 Energy Res 2015;3:00047. https://doi.org/10.3389/fenrg.2015.00047.

537 [7] Markides, CN. The role of pumped and waste heat technologies in a high-efficiency
538 sustainable energy future for the UK. Appl Therm Eng 2013;53:197-209.

539 [8] Li G, Shittu S, Diallo TMO, Yu M, Zhao X, Ji J. A review of solar photovoltaic-
540 thermoelectric hybrid system for electricity generation. Energy 2018;158:41–58.
541 https://doi.org/10.1016/J.energy.2018.06.021.

542 [9] Sark WGJHM van. Feasibility of photovoltaic - Thermoelectric hybrid modules. Appl
543 Energy 2011;88:2785–90. https://doi.org/10.1016/j.apenergy.2011.02.008.

544 [10] Zhu W, Deng Y, Wang Y, Shen S, Gulfam R. High-performance photovoltaic-
545 thermoelectric hybrid power generation system with optimized thermal management.
546 Energy 2016;100:91–101. https://doi.org/10.1016/j.energy.2016.01.055.

547 [11] Zhang J, Xuan Y. An integrated design of the photovoltaic-thermoelectric hybrid
548 system. Sol Energy 2019;177:293–8. https://doi.org/10.1016/j.solener.2018.11.012.

Preprint not peer reviewed

This preprint research paper has not been peer reviewed. Electronic copy available at: https://ssrn.com/abstract=6589681

549 [12] Rezania A, Sera D, Rosendahl LA. Coupled thermal model of photovoltaic-
550 thermoelectric hybrid panel for sample cities in Europe. Renew Energy 2016;99:127–
551 35. https://doi.org/10.1016/j.renene.2016.06.045.

552 [13] Motiei P, Yaghoubi M, GoshtashbiRad E, Vadiee A. Two-dimensional unsteady state
553 performance analysis of a hybrid photovoltaic-thermoelectric generator. Renew Energy
554 2018;119:551–65. https://doi.org/10.1016/j.renene.2017.11.092.

555 [14] Motiei P, Yaghoubi M, GoshtasbiRad E. Transient simulation of a hybrid photovoltaic-
556 thermoelectric system using a phase change material. Sustain Energy Techn Assess
557 2019;34:200–13. https://doi.org/10.1016/j.seta.2019.05.004.

558 [15] Bjørk R, Nielsen KK. The maximum theoretical performance of unconcentrated solar
559 photovoltaic and thermoelectric generator systems. Energy Convers Manag
560 2018;156:264–8. https://doi.org/10.1016/j.enconman.2017.11.009.

561 [16] Mahmoudinezhad S, Rezania A, Rosendahl LA. Behavior of hybrid concentrated
562 photovoltaic-thermoelectric generator under variable solar radiation. Energy Convers
563 Manag 2018;164:443–52. https://doi.org/10.1016/j.enconman.2018.03.025.

564 [17] Mahmoudinezhad S, Ahmadi Atouei S, Cotfas PA, Cotfas DT, Rosendahl LA, Rezania
565 A. Experimental and numerical study on the transient behavior of multi-junction solar
566 cell-thermoelectric generator hybrid system. Energy Convers Manag 2019;184:448–55.
567 https://doi.org/10.1016/j.enconman.2019.01.081.

568 [18] Rejeb O, Shittu S, Ghenai C, Li G, Zhao X, Bettayeb M. Optimization and performance
569 analysis of a solar concentrated photovoltaic-thermoelectric (CPV-TE) hybrid system.
570 Renew Energy 2020;152:1342–53. https://doi.org/10.1016/j.renene.2020.02.007.

571 [19] Rezania A, Rosendahl LA. Feasibility and parametric evaluation of hybrid concentrated
572 photovoltaic-thermoelectric system. Appl Energy 2017;187:380–9.
573 https://doi.org/10.1016/j.apenergy.2016.11.064.

574 [20] Rodrigo PM, Valera A, Fernández EF, Almonacid FM. Performance and economic
575 limits of passively cooled hybrid thermoelectric generator-concentrator photovoltaic
576 modules. Appl Energy 2019;238:1150–62.
577 https://doi.org/10.1016/j.apenergy.2019.01.132.

578 [21] Singh NK, Pandey J, Acharya S, Soni A. Charge carriers modulation and
579 thermoelectric performance of intrinsically p-type Bi_2Te_3 by Ge doping. J Alloys

This preprint research paper has not been peer reviewed. Electronic copy available at: https://ssrn.com/abstract=6589681

Compd 2018;746:350–5. https://doi.org/10.1016/j.jallcom.2018.02.310.

[22] Yin E, Li Q, Xuan Y. Feasibility analysis of a tandem photovoltaic-thermoelectric hybrid system under solar concentration. Renew Energy 2020;162:1828–41. https://doi.org/10.1016/j.renene.2020.10.006.

[23] Lekbir A, Hassani S, Ab Ghani MR, Gan CK, Mekhilef S, Saidur R. Improved energy conversion performance of a novel design of concentrated photovoltaic system combined with thermoelectric generator with advance cooling system. Energy Convers Manag 2018;177:19–29. https://doi.org/10.1016/j.enconman.2018.09.053.

[24] Gao Y, Dai Z, Wu D, Wang C, Chen B, Zhang X. Transient performance assessment of a hybrid PV-TEG system integrated with PCM under non-uniform radiation conditions: A numerical investigation. Renew Energy 2022;198:352–66. https://doi.org/10.1016/j.renene.2022.08.087.

[25] Rajaee F, Rad MAV, Kasaeian A, Mahian O, Yan WM. Experimental analysis of a photovoltaic/thermoelectric generator using cobalt oxide nanofluid and phase change material heat sink. Energy Convers Manag 2020;212:112780. https://doi.org/10.1016/j.enconman.2020.112780.

[26] Gao JL, Du QG, Zhang XD, Jiang XQ. Thermal stress analysis and structure parameter selection for a Bi 2Te 3-based thermoelectric module. J Electron Mater 2011;40:884–8. https://doi.org/10.1007/s11664-011-1611-3.

[27] Kolahan A, Maadi SR, Kazemian A, Schenone C, Ma T. Semi-3D transient simulation of a nanofluid-base photovoltaic thermal system integrated with a thermoelectric generator. Energy Convers Manag 2020;220:113073. https://doi.org/10.1016/j.enconman.2020.113073.

[28] Mattos LS, Scully SR, Syfu M, Olson E, Yang L, Ling C, et al. New Module Efficiency Record: 23.5% under 1-sun Illumination Using Thin-film Single-Junction GaAs Solar Cells. 2012 38th IEEE Photovoltaic Specialists Conference, Santa Clara: Alta Devices, Inc.; 2012, p. 3187–90.

[29] Essig S, Allebé C, Remo T, Geisz JF, Steiner MA, Horowitz K, et al. Raising the one-sun conversion efficiency of III-V/Si solar cells to 32.8% for two junctions and 35.9% for three junctions. Nat Energy 2017;2:171144. https://doi.org/10.1038/nenergy.2017.144.

Preprint not peer reviewed

This preprint research paper has not been peer reviewed. Electronic copy available at: https://ssrn.com/abstract=6589681

[30] Zhou J, Yi Q, Wang Y, Ye Z. Temperature distribution of photovoltaic module based on finite element simulation. Sol Energy 2015;111:97–103. https://doi.org/10.1016/j.solener.2014.10.040.

[31] Luo D, Wang R, Yu W, Zhou W. Parametric study of a thermoelectric module used for both power generation and cooling. Renew Energy 2020;154:542–52. https://doi.org/10.1016/j.renene.2020.03.045.

[32] Shittu S, Li G, Zhao X, Ma X, Akhlaghi YG, Fan Y. Comprehensive study and optimization of concentrated photovoltaic-thermoelectric considering all contact resistances. Energy Convers Manag 2020;205. https://doi.org/10.1016/j.enconman.2019.112422.

[33] Riahi A, Ben Haj Ali A, Fadhel A, Guizani A, Balghouthi M. Performance investigation of a concentrating photovoltaic thermal hybrid solar system combined with thermoelectric generators. Energy Convers Manag 2020;205:112377. https://doi.org/10.1016/j.enconman.2019.112377.

[34] Maxeon Solar Technologies. MAXEON 3 Solar Panel, cell type: SPR-MAX3-375-BLK.

[35] Jin Q, Jiang S, Zhao Y, Wang D, Qiu J, Tang DM, et al. Flexible layer-structured Bi_2Te_3 thermoelectric on a carbon nanotube scaffold. Nat Mater 2019;18:62–8. https://doi.org/10.1038/s41563-018-0217-z.

[36] Shin WH, Roh JW, Ryu B, Chang HJ, Kim HS, Lee S, et al. Enhancing Thermoelectric Performances of Bismuth Antimony Telluride via Synergistic Combination of Multiscale Structuring and Band Alignment by $FeTe_2$ Incorporation. ACS Appl Mater Interfaces 2018;10:3689–98. https://doi.org/10.1021/acsami.7b18451.

[37] Zhao L, He Y, Zhang H, Yi L, Wu J. Enhancing the thermoelectric property of Bi_2Te_3 through a facile design of interfacial phonon scattering. J Alloys Compd 2018;768:659–66. https://doi.org/10.1016/j.jallcom.2018.07.324.

[38] Zhang C, de la Mata M, Li Z, Belarre FJ, Arbiol J, Khor KA, et al. Enhanced thermoelectric performance of solution-derived bismuth telluride based nanocomposites via liquid-phase Sintering. Nano Energy 2016;30:630–8. https://doi.org/10.1016/j.nanoen.2016.10.056.

[39] Wang X yu, Wang H juan, Xiang B, Shang H jing, Zhu B, Yu Y, et al. Attaining reduced

Preprint not peer reviewed

This preprint research paper has not been peer reviewed. Electronic copy available at: https://ssrn.com/abstract=6589681

lattice thermal conductivity and enhanced electrical conductivity in as-sintered pure n-type Bi_2Te_3 alloy. J Mater Sci 2019;54:4788–97. https://doi.org/10.1007/s10853-018-3172-9.

[40] Chen S, Logothetis N, Ye L, Liu J. A High Performance Ag Alloyed Nano-scale n-type Bi_2Te_3 Based Thermoelectric Material. Mater Today Proc, vol. 2, Elsevier Ltd; 2015, p. 610–9. https://doi.org/10.1016/j.matpr.2015.05.083.

[41] An J, Han MK, Kim SJ. Synthesis of heavily Cu-doped Bi_2Te_3 nanoparticles and their thermoelectric properties. J Solid State Chem 2019;270:407–12. https://doi.org/10.1016/j.jssc.2018.11.024.

[42] Hirschberger M, Krizan JW, Cava RJ, Ong NP. Large thermal Hall conductivity of neutral spin excitations in a frustrated quantum magnet. Science (1979) 2015;348:106–9. https://doi.org/10.1126/science.1257340.

[43] Kato K, Hatasako Y, Uchino M, Nakata Y, Suzuki Y, Hayakawa T, et al. Flexible Porous Bismuth Telluride Thin Films with Enhanced Figure of Merit using Micro-Phase Separation of Block Copolymer. Adv Mater Interfaces 2014;1. https://doi.org/10.1002/admi.201300015.

[44] Shi W, Wu F, Wang K, Yang J, Song H, Hu X. Preparation and thermoelectric properties of yttrium-doped Bi_2Te_3 flower-like nanopowders. J Electron Mater 2014;43:3162–8. https://doi.org/10.1007/s11664-014-3220-4.

Preprint not peer reviewed

This preprint research paper has not been peer reviewed. Electronic copy available at: https://ssrn.com/abstract=6589681